PHILOSOPHICAL TRANSACTIONS OF THE ROYAL SOCIETY A MATHEMATICAL, PHYSICAL & ENGINEERING SCIENCES

On the Theory of Ring Spinning

W. B. Fraser

Phil. Trans. R. Soc. Lond. A 1993 **342**, 439-468
doi: 10.1098/rsta.1993.0028

On the theory of ring spinning†

By W. B. Fraser

School of Mathematics and Statistics, The University of Sydney, New South Wales 2006, Australia

Contents

The mathematical model for balloon formation in the ring spinning process has been well established since the mid-1950s. The availability of present day computational power has made it possible to carry out a comprehensive analysis of the equations which it is hoped will give fresh insight into the physics of ring spinning.

This paper is mainly concerned with free balloon spinning (without control rings). The relation between guide eye tension and traveller mass is explored in detail and an important transition region in this dependence is identified. The dependence of this transition region on bobbin radius, balloon height and air drag

† This paper was produced from the author's disk by using the TEX typesetting system.

Phil. Trans. R. Soc. Lond. A (1993) **342**, 439–468
Printed in Great Britain

is also examined in detail. The practical application of the theory is discussed and theoretical minimum traveller mass against balloon height curves are produced. The results of a simulation of one traverse of the ring rail up and down the conical chase of a cop-structured bobbin is presented. Finally, the theory is modified to allow for the presence of a control ring and results that show the effect of the control ring on the guide eye tension against traveller mass dependence are presented.

1. Introduction

Spinning is the final step in the manufacture of yarn from staple fibres after which the spun yarn is wound onto a bobbin or package. After a process of combing and drafting, that aligns the fibres into a soft strand of the desired linear density called a *roving*, the ring spindle (figure 1) simultaneously twists the yarn and winds it onto a bobbin mounted on a driven spindle. The ring spinning frame was invented by the American John Thorp in 1828. In the preface to his 1987 book Klein estimated that there were at that time 160 million ring spindles in operation throughout the world. In emphasizing the importance of this method of yarn production Klein has this to say:

'. . . the ring frame has a very great influence on the yarn product and its quality. Ring-spun yarn still provides the absolute standard of comparison in evaluation of yarns formed by other spinning processes.'

A detailed description of the operation of a modern ring spinning frame and some account of the history of its development can be found in Klein's book and also more extensively in de Barr & Catling (1965, ch. 2). Only a brief description will be given here.

The modern ring spinning frame consists of many vertically mounted spindles with a train of drafting rollers above each spindle. A roving package is mounted above each spindle position and the roving is first led through this final drafting train which reduces it to the required fineness before spinning. The yarn issuing from the front rollers D (figure 1) passes through a guide eye O located axially above the spindle S. From the guide eye the yarn passes around the traveller T, which is free to rotate around the ring R. From T it passes to the wind-on or lay point L where it is wound onto the bobbin B carried on the spindle which is coaxial with the ring. The spindle is driven at a constant angular speed ω_0 (rad s^{-1}) and the traveller is dragged around the ring by the loop of yarn OTL. When the drafting rollers are stationary, the angular speed of the traveller is the same as that of the spindle and each revolution of the spindle causes one turn of twist to be inserted in the loop of yarn between the front roller nip and the traveller. However, if the yarn is issuing from the front rollers at a speed V (m s^{-1}) and is also being wound onto the bobbin, the angular speed ω (rad s^{-1}) of the traveller is less than that of the spindle and this difference in angular speed is related to V by the equation

$$\omega_0 - \omega = V/b, \tag{1.1}$$

where b is the radius of the bobbin at the lay point L. In this equation the angular speed of the spindle is very much greater than the yarn delivery speed V so that

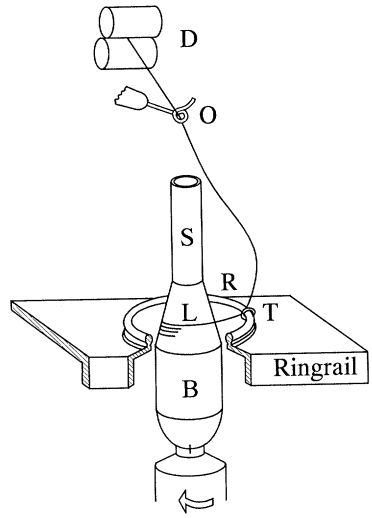

Figure 1. The ring spinning spindle.

for all practical purposes the angular speed of the traveller can be taken to be the same as that of the spindle (de Barr & Catling 1965, eqn (2.1)). The surface generated by the rotating loop of yarn between the guide eye and the traveller is called a balloon. A knowledge of the balloon dimensions and the yarn tensions in the balloon is extremely important for the design and efficient operation of ring spinning frames. Similar balloons also occur during the high speed over-end unwinding of large packages and these have been investigated by Padfield (1958), Kothari & Leaf (1979) and Fraser *et al.* (1992).

Yarn is twisted to give it tensile strength and the tension at which twist insertion (spinning) is carried out is critical. Tension during spinning must not exceed the strength of the yarn at any instant. On the other hand it is necessary to spin at a high enough tension to prevent balloon collapse which can result in the yarn becoming wrapped around the spindle which also causes yarn breaks. At a more subtle level, the tension at which the yarn is formed influences its structure and properties. Finally the power consumed in the spinning process is proportional to the product of the lay-point yarn tension and the spindle speed so that it is necessary to balance operating conditions to minimize power consumption while maximizing yarn production. The parameters that spinners operating a given ring frame have at their disposal to control tension and achieve optimal spinning are the spindle speed, the yarn delivery speed V and the traveller mass. The theoretical model described in this paper offers operators the possibility of achieving this more effectively.

The theory of ring spinning, which is the theory of the thread-line dynamics between the guide eye and the lay point, has a long history starting with a paper by Lüdicke (1881). An account of this history with references up to 1965 can be found in de Barr & Catling (1965), where a comprehensive account of the state of the theory at that time can also be found. By 1965 the equations of motion for the thread line in the balloon and the equations of motion for the traveller were well known. There is also a secondary balloon between the traveller and the lay point but as this distance is quite small the thread line is usually assumed to

follow a straight path from T to L and the tension is assumed constant (de Barr & Catling 1965, § 5.2; Batra *et al.* 1989*a*). The relative importance of the air drag and the centripetal and Coriolis acceleration terms in the balloon equations was understood and in the 1950s some limited numerical solutions of these equations were obtained. However, the use of the traveller mass equations to formulate a complete set of boundary conditions for the balloon equations at the ring was not fully exploited at this time.

Recent advances in the technology of ring spinning machinery linked with the enormous increase in computing power since 1965 has generated a renewed interest in this problem. The papers of Batra *et al.* (1989*a*–*c*) reflect the current state of the theory and contain references to other work up to the present. Even in this most recent work the use of the traveller mass equations as a boundary condition on the balloon equations has not been fully exploited.

It is the purpose of the present paper to present a complete theoretical and numerical study of the way in which guide eye tension depends on traveller mass and spindle speed. This is possible when the balloon boundary condition derived from the equations of motion for the traveller mass is fully exploited in the computational algorithm. This dependence turns out to be complex (figures 3*a*, 4*a*, 5*a*) as is to be expected given the nonlinear nature of the problem. However, it will be shown that these results can be used to identify ranges of operating conditions (spindle speed/traveller mass) that would result in balloon instability and graphs showing the minimum traveller mass required to prevent balloon collapse as a function of balloon height are presented. These theoretical results are in general agreement with the results in de Barr & Catling (1965, ch. 15).

All of these results are for free balloon spinning (without control rings) as it seems best to present the basic results and physical insights free from the additional complexity introduced by the presence of control rings. However, all modern spinning machines use one or more control rings to restrict the balloon diameter and reduce the yarn tension at high spindle speeds. In the final section of the paper the theory is modified to include the presence of control rings and results are presented for the case of a single control ring located at the midpoint of the balloon height.

The plan of the paper is as follows. In the next section the equations of motion for the yarn in the balloon and the traveller mass will be reviewed and the two-point boundary value problem for the shape of the yarn in the balloon without control rings will be formulated. These equations will then be cast in a dimensionless form that minimizes the number of parameters in the problem and which also brings out clearly the relative importance of the various terms in the equations. In § 3 the numerical method used for solving this boundary value problem is described. In § 4 the dependence of guide eye tension on traveller mass is investigated in detail. In the first part of this section results for a balloon of height $h = 10a$ and lay-point radius $b = 0.5a$, where a is the traveller ring radius, are presented for a very large range of traveller mass parameter. An important transition region in this relationship is identified: the range of (increasing) traveller mass values over which the balloon profiles change from stable, low tension, two-loop shapes to stable, higher tension, single-loop shapes. In the second part of § 4 the dependence of this transition region on balloon height, lay point radius and air drag parameter is investigated.

The practical application of the theory is discussed in § 5, where theoretical minimum traveller mass against balloon height curves are presented and compared with the minimum traveller mass formula given by de Barr & Catling (1965). The result of a simulation of one traverse of the ring rail up and down the conical chase of a cop-structured bobbin is also presented. In § 6 the theory is modified to allow for the presence of a control ring and results that show the effect of the control ring on the guide eye tension against traveller mass dependence are presented.

2. The mathematical formulation

The equations describing the motion of yarn as it passes through a ring spinning device are by now well established and a detailed derivation can be found in the book by de Barr & Catling (1965). Before proceeding to review the derivation it is appropriate to review the assumptions that are customarily made in the derivation.

(*a*) *The assumptions*

1. The yarn is assumed to be inextensible, perfectly flexible and of uniform density and cross section so that only tension forces act in the yarn. The effect of yarn elasticity on balloon shape and tension in over-end unwinding has been investigated in a recent paper (Fraser 1992), where it has been shown that this effect is very small for typical unwinding tensions. It has also been found that the effect is small in the case of the tensions encountered in ring spinning. In this paper inextensible yarn will be assumed throughout. The effect of gravity on the yarn in the balloon will also be neglected. The effect of gravity on tension and balloon shape in an unwinding balloon has been investigated by Kothari & Leaf (1979*a*). They found that changes in maximum balloon radius and guide eye tension were less than 3% for all cases investigated.

2. The yarn path between the traveller and the lay point on the bobbin is assumed to be a straight line (i.e. air drag is neglected on this short section of the yarn) and the lay point is assumed to lie in the plane of the traveller ring.

3. Since the motion of the ring rail and the rate at which the balloon height changes as the yarn layers are built up on the bobbin is very slow compared with the rotational speed of the loop of yarn in the balloon the time-dependent terms in the equations of motion will be neglected; i.e. the balloon shape is assumed stationary relative to a frame of reference rotating with the same (constant) angular speed as the traveller mass. A perturbation scheme (Kevorkian & Cole 1981) could of course be used to formalize this assumption as was done for the case of balloon formation in yarn unwinding over-end from a helically wound package (Fraser *et al.* 1992). This will not be investigated further here as the difference in the timescales involved is even greater than in the unwinding problem.

4. It will be shown that when the equations of motion for the yarn in the balloon are written in dimensionless form the terms involving the yarn speed V, such as the Coriolis acceleration terms, can be neglected. The effect of air drag on balloon shape cannot be neglected and the assumptions made in the model of air drag used here are discussed in § 4 *b*(i).

5. In the derivation of the equations of motion for the traveller it is treated as a point mass and Amonton's law of friction will be used to model the interaction

between the traveller and the ring and the yarn and the traveller. The weight of the traveller will also be neglected as this force is small compared with the yarn tension and the frictional and dynamical forces acting on the traveller.

6. The numerical and graphical results presented in this paper have been calculated for only one value of the coefficient of ring/traveller and traveller/yarn friction assuming a constant wrap angle of the yarn on the traveller. The wrap angle depends on the direction of the yarn tangents on either side of the traveller and on the ratio of the radius of the bobbin b at the lay point to the traveller ring radius a. As the yarn layers are built up on the bobbin this ratio changes periodically with the oscillatory motion of the traveller ring rail. Again the rate of change of the value of b/a will be slow compared with the rotational speed of traveller.

In practice these variations in balloon height and lay-point radius with time are very significant as they cause variations in the yarn tension throughout the building of the bobbin which are undesirable. The solution of the time-dependent problem can be constructed from a sequence of stationary balloon solutions for an appropriate range of balloon heights and bobbin radius in the same way that the time-dependent solution of the over-end unwinding problem was obtained (Fraser *et al.* 1992). An example of how the theory can be used to simulate the variations in the balloon profile and tension as the ring rail moves from the bottom to the top of the conical chase winding one layer of yarn onto a cop-structured bobbin is given in § 5. In the next two subsections the derivation of the equations of motion for the yarn in the balloon and the traveller mass will be reviewed.

(*b*) *The equations for the yarn in the balloon*

Consider a material point P (figure 2) of the yarn which at time t is a distance s measured along the yarn from the guide eye. Let $\boldsymbol{R}(s,t) = r\boldsymbol{e}_r + z\boldsymbol{k}$, be the position vector of P relative to an origin of coordinates at the guide eye O (figure 2). Let r, θ, z be cylindrical coordinates corresponding to unit base vectors $\boldsymbol{e}_r$, $\boldsymbol{e}_\theta$, $\boldsymbol{k}$ of a coordinate system that rotates with a constant angular velocity $\omega\boldsymbol{k}$ about the z-axis, which coincides with the axis of the spindle. The direction of the z-axis is positive down towards the bobbin and ω is the angular speed of the traveller.

If $T(s,t)$ is the tension in the yarn at P then the full vector form of the time-dependent equation of motion for the yarn element at P is

$$m\left\{D^2\boldsymbol{R} + 2\omega\boldsymbol{k}\wedge D\boldsymbol{R} + \omega^2\boldsymbol{k}\wedge(\boldsymbol{k}\wedge\boldsymbol{R})\right\} = \frac{\partial}{\partial s}\left(T\frac{\partial\boldsymbol{R}}{\partial s}\right) + \boldsymbol{F}, \tag{2.1}$$

where m is the linear density of the yarn. The differential operator D is given by

$$D = \frac{\partial}{\partial t} + V\frac{\partial}{\partial s},$$

where V is the constant linear speed at which the thread line issues from the final drafting rollers (D, figure 1). However, by Assumption 3 above the solution relative to the rotating coordinate system is independent of time so that the operator D reduces to

$$D = V\frac{\mathrm{d}}{\mathrm{d}s}. \tag{2.2}$$

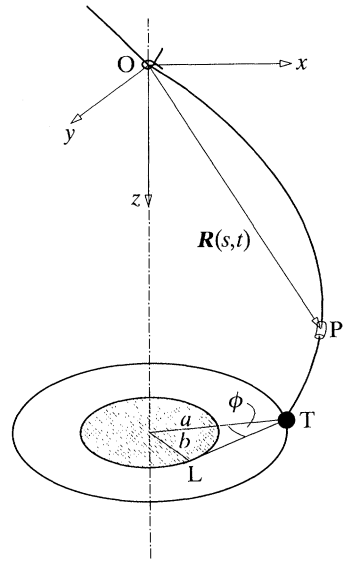

Figure 2. The thread line.

From now on steady-state conditions will be assumed. Equation (2.1) is by now well established and the details of its derivation can be found in de Barr & Catling (1965, ch. 4) and also in Batra *et al.* (1989*a*). The operator D is the total time derivative following the motion of P relative to the rotating frame. Thus $D\boldsymbol{R}$ is the velocity of the material particle P and $D^2\boldsymbol{R}$ is its acceleration relative to the rotating frame. The second term in the braces on the left-hand side of equation (2.1) is the Coriolis acceleration of P. The vector $\boldsymbol{F}$ is the air drag force per unit length acting on the yarn in the balloon.

A detailed discussion of air drag and its effect on balloon shape and tension in ring spinning processes can be found in de Barr & Catling (1965, ch. 3), Kothari & Leaf (1979*a*) and Batra *et al.* (1989*b*). Only the component of air drag normal to the yarn will be considered here. Thus, if $\boldsymbol{v}_{\mathrm{n}}$ is the normal component of the yarn velocity at P, the air drag force vector is given by

$$\boldsymbol{F} = -D_{\mathrm{n}}|\boldsymbol{v}_{\mathrm{n}}|\boldsymbol{v}_{\mathrm{n}}, \tag{2.3}$$

where

$$\begin{aligned}\boldsymbol{v}_{\mathrm{n}} &= \boldsymbol{v} - \left(\boldsymbol{v}\cdot\frac{\mathrm{d}\boldsymbol{R}}{\mathrm{d}s}\right)\frac{\mathrm{d}\boldsymbol{R}}{\mathrm{d}s}\\ &= \frac{\mathrm{d}\boldsymbol{R}}{\mathrm{d}s}\wedge\left(\boldsymbol{v}\wedge\frac{\mathrm{d}\boldsymbol{R}}{\mathrm{d}s}\right),\end{aligned} \tag{2.4}$$

and

$$\boldsymbol{v} = D\boldsymbol{R} + \omega\boldsymbol{k}\wedge\boldsymbol{R}. \tag{2.5}$$

The well-known vector identity for the triple vector product has been used to deduce the second expression for $\boldsymbol{v}_{\mathrm{n}}$ above. The air drag coefficient D_{n} has been discussed by Fraser *et al.* (1991) and its magnitude in the ring spinning situation will be discussed in § 2*f* below.

The vector differential equation (2.1) represents three-component equations for

the four unknown functions $r(s)$, $\theta(s)$, $z(s)$ and $T(s)$. The fourth equation that completes the system is given by the inextensibility condition:

$$\frac{\mathrm{d}\boldsymbol{R}}{\mathrm{d}s} \cdot \frac{\mathrm{d}\boldsymbol{R}}{\mathrm{d}s} = 1. \tag{2.6}$$

(c) *The equations for the motion of the traveller*

The forces acting on the traveller will be denoted as follows: T_1 is the yarn tension on the balloon side of the traveller; T_2 is the yarn tension on the bobbin side of the traveller; $\boldsymbol{N} = N_r\boldsymbol{e}_r + N_z\boldsymbol{k}$ is the force the ring exerts on the traveller in the direction normal to the ring; $-\mu\sqrt{N_r^2 + N_z^2}\,\boldsymbol{e}_\theta$ is the frictional drag that the ring exerts on the traveller, where μ is the coefficient of ring/traveller friction.

As noted above (Assumption 5) the effect of gravity on the traveller will be neglected so that the vector form of the equation of motion for a traveller of mass m_T in circular motion (radius a) with constant angular speed ω is

$$-m_\mathrm{T}\omega^2 a\boldsymbol{e}_r = -T_1 \left.\frac{\mathrm{d}\boldsymbol{R}}{\mathrm{d}s}\right|_{s_1} - T_2\cos\phi\,\boldsymbol{e}_r + T_2\sin\phi\,\boldsymbol{e}_\theta + \boldsymbol{N} - \mu|\boldsymbol{N}|\boldsymbol{e}_\theta. \tag{2.7}$$

The angle ϕ ($\sin\phi = b/a$) is the angle the yarn between the traveller and the lay point makes with the radial direction (figure 2), s_1 is the length of yarn in the balloon between the guide eye and the traveller and $(\mathrm{d}\boldsymbol{R}/\mathrm{d}s)|_{s_1}$ is the unit tangent vector to the yarn in the balloon at the traveller.

The r, θ and z components of this equation are, respectively,

$$-m_\mathrm{T}\omega^2 a = -T_1 r'(s_1) - T_2\cos\phi + N_r, \tag{2.8}$$

$$0 = -T_1 a\theta'(s_1) + T_2\sin\phi - \mu\sqrt{N_r^2 + N_z^2}, \tag{2.9}$$

$$0 = -T_1 z'(s_1) + N_z, \tag{2.10}$$

where $(\,)' \equiv (\mathrm{d}/\mathrm{d}s)(\,)$. These equations correspond to eqs (18)–(21) in the paper by Crank (1953)

Tensions T_1 and T_2 are in fact the tensions at either end of a small but finite yarn segment contacting the traveller wire and rubbing against it. Their magnitudes are related by Euler's equation for tension variation in a string passing around a rough cylinder:

$$T_2 = T_1 \mathrm{e}^{\mu_y\alpha} = gT_1, \tag{2.11}$$

where μ_y is the coefficient of friction between the yarn and the traveller, α is the angle of wrap and $g = \exp(\mu_y\alpha)$ is the traveller yarn friction parameter introduced by Batra *et al.* (1989*a*, eqn (23)).

It will now be shown that these equations provide one of the boundary conditions on the balloon equations (2.1)–(2.6) at the traveller.

(d) *Formulation of the boundary conditions*

The balloon equations must be solved subject to boundary conditions at each end of the yarn in the balloon, at the guide eye and at the traveller ring.

(i) *At the guide eye*

The boundary condition at the guide eye which is at the origin of the coordinate system is simply that at $s = 0$

$$\boldsymbol{R}(0) = \mathbf{0}, \qquad \text{i.e.} \quad r(0) = 0, \quad z(0) = 0. \tag{2.12}$$

Because of the rotational symmetry of the problem $\theta(s)$ is only determined to within an additive arbitrary constant so that $\theta(0)$ can be set equal to zero without loss of generality.

(ii) *At the traveller*

Let h be the height of the guide eye above the traveller ring and $s = s_1$ be the length of yarn in the balloon so that the geometrical boundary conditions at the traveller are

$$r(s_1) = a, \quad z(s_1) = h. \tag{2.13}$$

The other boundary condition is obtained from the traveller equations (2.8)–(2.11) as follows. First use (2.11) to eliminate T_2 from the other three equations and then eliminate N_z between (2.9) and (2.10) to obtain

$$\mu^2 \left\{ N_r^2 + [T_1 z'(s_1)]^2 \right\} = T_1^2 \left[a\theta'(s_1) - g \sin\phi \right]^2. \tag{2.14}$$

Finally eliminate N_r between (2.8) and (2.14) to obtain the dynamical boundary condition at the traveller.

$$T_1[g \sin\phi - a\theta'(s_1)] = \mu \sqrt{\{T_1[r'(s_1) + g\cos\phi] - m_{\mathrm{T}}\omega^2 a\}^2 + T_1^2 z'(s_1)^2}. \tag{2.15}$$

This condition relates the yarn tension at the bottom of the balloon T_1 and the traveller mass m_{T} to the geometrical quantities $r'(s_1)$, $\theta'(s_1)$, $z'(s_1)$, ϕ, and the friction parameters μ and g.

Equation (2.15) corresponds to Crank (1953, eqn (22)), Shantong (1987, eqn (3)) and Batra *et al.* (1989*a*, eqn (28)). However, these authors do not exploit this boundary condition on the balloon equations to the fullest possible extent, stopping short of a full exploration of the solution space of the equations.

In the more complete investigation of the solution space presented here it will be shown that there are certain ranges of traveller mass values for which the solutions of the balloon equations cease to be unique. These triple solution regions will be identified with conditions that lead to dynamically unstable balloons. Thus, the more extensive exploration of the solution space given in this paper provides considerable new insights into the physics of ring spinning and also provides the mathematical basis for programming the speed of individually driven spindles to achieve optimal bobbin build.

This completes the mathematical formulation of the ring spinning problem.

(*e*) *The dimensionless equations*

In this section all variables will be scaled against length and force scales appropriate to the ring spinning problem and the above equations will be rewritten in dimensionless form. Some researchers (Crank 1953; Nerli *et al.* 1980; Lisini *et al.* 1981) have been reluctant to present their results in terms of dimensionless variables feeling that results expressed in dimensional variables are more accessible to the industrial technical community. The more mathematically orientated authors

(e.g. Padfield 1958; Batra *et al.* 1989) express their results in dimensionless variables. The importance of dimensional analysis in scientific research can hardly be over emphasized and the reader is referred to the books by Bridgeman (1931), Sedov (1959), and more recently Bluman & Kumei (1989), to list but a few. The considerable advantages to be obtained from a dimensionless presentation of results for the present problem are listed below.

1. The guide eye tension T_0 and balloon profile depend on a large number of independent variables such as the friction parameters μ, g, balloon height and radius (h, a), traveller speed ωa and yarn speed V (which are related to the angular speed of the spindle ω_0 by equation (1.1)), the linear density of the yarn m and the traveller mass m_{T}. A considerable reduction in the number of these independent variables can be achieved if they are collected together in dimensionless groups.

2. The value of the dimensionless coefficients multiplying each of the terms in the dimensionless form of the very general equation (2.1) can be estimated for typical spinning conditions. This gives an indication of the relative importance of each term and in particular it will be shown that the Coriolis acceleration term and the operator D can be set to zero without significant loss of computational accuracy. On the other hand it will be seen that the air drag term cannot be neglected.

3. Results obtained from dimensionless equations are more general and apply to a range of particular spinning conditions. This leads to savings in the computational effort and a more economical graphical and tabular presentation of results.

4. From such general results it is easier to reach theoretical and physical interpretations of phenomena observed experimentally and in ring-spinning practice. For example the balloon instability for certain ranges of spindle speed reported in Platt's Bulletin (1955, vol. 9) are at least qualitatively explained in terms of the results given in this paper.

The dimensionless variables used here are the same as those used by Padfield (1958, eqs (5)) and similar to those used by Fraser *et al.* (1992, eqs (18)) except that tension and force are scaled against $m\omega^2 a^2$ and velocity is scaled against ωa in the present paper rather than mV^2 and V, respectively, which was appropriate for the unwinding problem. Batra *et al.* (1989) use balloon height h to scale the z coordinate, traveller ring radius a to scale the r coordinate and scale tension and force against the guide eye tension T_0. This leads to a somewhat less convenient set of dimensionless parameters but, where appropriate for comparison, the conversion relation between their parameters and those used in this paper will be given.

Thus the following dimensionless variables will be introduced, and in these definitions barred variables are dimensionless:

$$\left.\begin{aligned} \bar{\boldsymbol{R}} = \frac{\boldsymbol{R}}{a} = \frac{r}{a}\boldsymbol{e}_r + \frac{z}{a}\boldsymbol{k} = \bar{r}\boldsymbol{e}_r + \bar{z}\boldsymbol{k}, \\ \bar{s} = \frac{s}{a}, \quad \bar{\boldsymbol{v}}_{\mathrm{n}} = \frac{\boldsymbol{v}_{\mathrm{n}}}{\omega a}, \quad \bar{\boldsymbol{v}} = \frac{\boldsymbol{v}}{\omega a}, \quad \bar{T} = \frac{T}{m\omega^2 a^2}, \quad \bar{\boldsymbol{F}} = \frac{\boldsymbol{F}}{m\omega^2 a}. \end{aligned}\right\} \tag{2.16}$$

Expressed in terms of these dimensionless variables equation (2.1) becomes

$$\Omega^{-2}\frac{\mathrm{d}^2\bar{\boldsymbol{R}}}{\mathrm{d}\bar{s}^2}+2\Omega^{-1}\frac{\mathrm{d}\bar{\boldsymbol{R}}}{\mathrm{d}\bar{s}}+\boldsymbol{k}\wedge(\boldsymbol{k}\wedge\bar{\boldsymbol{R}})=\frac{\mathrm{d}}{\mathrm{d}\bar{s}}\left(\bar{T}\frac{\mathrm{d}\bar{\boldsymbol{R}}}{\mathrm{d}\bar{s}}\right)+\bar{\boldsymbol{F}}, \tag{2.17}$$

where

$$\Omega=\omega a/V \tag{2.18}$$

is the angular velocity parameter defined in Fraser *et al.* (1992, eqn (21)).

The dimensionless form of the air drag term, equations (2.3)–(2.5), is

$$\bar{\boldsymbol{F}}=-\tfrac{1}{16}p_0|\bar{\boldsymbol{v}}_\mathrm{n}|\bar{\boldsymbol{v}}_\mathrm{n},\quad \bar{\boldsymbol{v}}_\mathrm{n}=\frac{\mathrm{d}\bar{\boldsymbol{R}}}{\mathrm{d}\bar{s}}\wedge\left(\bar{\boldsymbol{v}}\wedge\frac{\mathrm{d}\bar{\boldsymbol{R}}}{\mathrm{d}\bar{s}}\right),\quad \bar{\boldsymbol{v}}=\Omega^{-1}\frac{\mathrm{d}\bar{\boldsymbol{R}}}{\mathrm{d}\bar{s}}+\boldsymbol{v}k\wedge\bar{\boldsymbol{R}}, \tag{2.19}$$

and the air drag coefficient

$$p_0=16D_\mathrm{n}a/m \tag{2.20}$$

is the same as the air drag coefficient introduced by Padfield (1958) and used by Fraser *et al.* (1992) and Fraser (1992).

Finally the dimensionless forms of the boundary conditions (2.12), (2.13) and (2.15) are, respectively,

$$\bar{r}(0)=0,\quad \bar{z}(0)=0,\quad \theta(0)=0, \tag{2.21}$$

$$\bar{z}(\bar{s}_1)=\bar{h}=h/a,\quad \bar{r}(\bar{s}_1)=1, \tag{2.22}$$

$$\bar{T}_1[g\sin\phi-\theta'(\bar{s}_1)]=\mu\sqrt{[\bar{T}_1(\bar{r}'(s_1)+g\cos\phi)-M]^2+[\bar{T}_1\bar{z}'(\bar{s}_1)]^2}, \tag{2.23}$$

where

$$M=m_\mathrm{T}/ma. \tag{2.24}$$

is the dimensionless traveller mass parameter which is the ratio of the traveller mass to the mass of a segment of yarn equal in length to traveller ring radius a.

(*f*) *The magnitude of the parameters* Ω *and* p_0

From the dynamical point of view the angular speed of the spindle ω_0 is independent of the yarn speed V which is controlled by the front rollers of the drafting train (D in figure 1). Practically, of course, the relationship between these two quantities is determined by the amount of twist that is being inserted in the yarn. Typically, spindle speed ω_0 is very large compared with the front roller speed so that the angular speed of the traveller ω is not very different from the spindle speed equation (1.1). The difference in speeds is just enough to allow for the desired amount of twist insertion in the yarn. Thus $\omega a\gg V$ and Ω is a large parameter.

Typical values of Ω can be calculated from data given in Batra *et al.* (1989*c*, Table 1) where in their notation

$$\Omega=2P^2/K.$$

They use a range of values from $\Omega=75$ to $\Omega=200$ for their calculations. These values are consistent with the range of values calculated from cotton spinning data suppplied by Dr N. Johnson of the School of Fibre Science and Technology, University of New South Wales.

The first two terms on the left side of (2.17) are multiplied by Ω^{-2} and Ω^{-1}, respectively, so that the order of magnitude of the first term is typically 2.5–16.9×10^{-5}, while that of the second term, which is the Coriolis acceleration term, is 5–13×10^{-3}. Thus in many spinning situations the first two terms on the left of (2.17) can be neglected without significant loss of accuracy and from now on the spinning balloon equation will be taken as

$$\boldsymbol{k}\wedge(\boldsymbol{k}\wedge\bar{\boldsymbol{R}})=\frac{\mathrm{d}}{\mathrm{d}\bar{s}}\left(\bar{T}\frac{\mathrm{d}\bar{\boldsymbol{R}}}{\mathrm{d}\bar{s}}\right)+\boldsymbol{F}. \tag{2.25}$$

This is in contrast to the unwinding problem where the angular speed of the loop of yarn in the balloon and the unwinding withdrawal speed V are intimately connected through the package wind-on angle (Fraser *et al.* 1992). In this case $\Omega\approx1$ and the first two terms on the left of the balloon equation must be retained.

Since the order of magnitude of the scaled normal velocity $\bar{\boldsymbol{v}}_{\mathrm{n}}$ is unity the magnitude of the air drag term is determined by the order of magnitude of the parameter $\frac{1}{16}p_0$. The method for calculating this parameter is described by Batra *et al.* (1989*b*, Table 1) and in their notation

$$\tfrac{1}{16}p_0=aD_{\mathrm{n}}/m=Q^2/P^2.$$

In their calculations they use a range of values of Q^2/P^2 from 0.26 to 0.50, which gives $p_0=4.16$–8.07 and this is the range of p_0 that will be used here.

It is clear that air drag plays a significant part in balloon formation in both ring spinning and unwinding and that the air drag term cannot be omitted from the equations of motion. Other aspects of the approximations made in considering only the normal component of air drag to be important are discussed by Kothari & Leaf (1979*a*) and Batra *et al.* (1989*b*), where further references can be found.

In the remainder of this and the next section all variables will be dimensionless so that the bar over the dimensionless variables will be omitted. However, in § 4, where the results are discussed, and for the labels on the graphs it is convenient to revert to dimensional quantities.

(*g*) *Derivation of the tension equation*

To derive the tension equation: form the scalar product of equation (2.25) with $\mathrm{d}\boldsymbol{R}/\mathrm{d}s$ and observe that differentiation of equation (2.6) gives

$$\frac{\mathrm{d}\boldsymbol{R}}{\mathrm{d}s}\cdot\frac{\mathrm{d}^2\boldsymbol{R}}{\mathrm{d}s^2}=0,$$

and since the air drag is normal to the yarn

$$\frac{\mathrm{d}\boldsymbol{R}}{\mathrm{d}s}\cdot\boldsymbol{F}=0.$$

When use is made of the above and after some rearrangement the final result is

$$\frac{\mathrm{d}T}{\mathrm{d}s}=\frac{\mathrm{d}}{\mathrm{d}s}(\tfrac{1}{2}r^2). \tag{2.26}$$

Equation (2.26) can be integrated to give the following expression for the tension as a function of guide eye tension T_0 and balloon radius $r(s)$:

$$T(s)=T_0-\tfrac{1}{2}r^2. \tag{2.27}$$

This is an exact first integral of the equations of motion. The balloon profile and the value of T_0 must be obtained by numerical integration of (2.25) subject to the boundary conditions (2.21)–(2.23).

3. Method of numerical solution

The numerical solution of equations (2.25) and (2.6) with the tension T given by equation (2.27) and subject to boundary conditions (2.21)–(2.23) is fairly straight forward and will only be described briefly. First notice that this problem is rather like a nonlinear eigenvalue problem with guide eye tension T_0 as the eigenvalue. Thus T_0 is to be determined as part of the solution together with the coordinate functions $r(s)$, $\theta(s)$, $z(s)$ and the length s_1 of yarn in the balloon between the guide eye and the traveller. Second, the vector equation (2.25) has to be resolved into its three component differential equations. The cylindrical and cartesian coordinate components of equation (2.25) are given in the appendix. The inextensibility condition equation (2.6) has been used up in the derivation of the tension equation (2.27) so that the three second-order differential equations (A 1)–(A 3), or alternatively (A 6)–(A 8), subject to six boundary conditions (2.21)–(2.23) constitute a well-posed problem for the determination of the three coordinate functions.

The shooting method for the numerical solution of two-point boundary value problems (Press *et al.* 1986, § 16.1) was used to obtain the results presented in this paper.

The procedure, as it applies to the cylindrical component equations, is to solve equations (A 1)–(A 3) as an initial value problem subject to initial conditions $r = \theta = z = 0$ at $s = 0$ with prescribed trial values of T_0 and $r'(0)$, which lead to

$$z'(0) = \sqrt{1 - r'(0)^2},$$

by the inextensibility condition, and $\theta'(0) = 0$ by equation (A 5_2) in the appendix. A fifth-order Runge–Kutta routine is used to solve this initial value problem and the integration is stopped when $z(s) = h$, the prescribed balloon height. (This determines s_1.) A Newton–Raphson type scheme is used to adjust the values of T_0 and $r'(0)$ until the other two boundary conditions (2.22_2) and (2.23) at the traveller are satisfied. Thus the guide eye tension T_0 and the initial slope $r'(0)$ are determined as part of the solution. The partial derivatives of the trial solutions with respect to T_0 and $r'(0)$ required in the Newton–Raphson iteration are calculated numerically.

Only a minor modification of the above procedure is required if the cartesian component equations are used instead of the cylindrical component equations. In fact for computational purposes the cartesian equations are a more balanced set of equations. This can be seen by inspection of the power series solutions in the neighbourhood of the origin which are given in equations (A 5) and (A 10). Component functions $x(s)$, $y(s)$, $z(s)$ start off proportional to s, whereas $\theta(s)$ increases very slowly (as s^3) which can lead to numerical problems. The cartesian equations were used in the computation of all the results to be presented below. The convergence of the shooting method algorithm was very fast even for trial values of T_0 up to 10% away from the converged value. The initial slope value $r'(0) = 0.5$ was used to initiate all calculations. For ranges of traveller mass

parameter $M = m_T/ma$ where multiple solutions exist a more careful choice of trial initial conditions was necessary to ensure convergence to the required solution.

The values of the friction parameters used for all calculations were $\mu = 0.1$, $g = \exp(\mu_y \alpha) = 1.7$ (these are the values used by Batra *et al.* (1989)). The value of the air drag parameter used for most of the calculations was $p_0 = 4.0$, which is in the range used by Batra. However, as explained below, the form of the guide eye tension against traveller mass curves in the important C–D transition range (figures 4*a*, 6*a*, *b*) turns out to be sensitive to variation in the value of p_0 and this is discussed in § 4 *b*(i).

The calculations were carried out for a large range of traveller mass parameter values: $0 \leq M \leq 1000$. The results have been used to construct curves that show the dependence of guide eye tension parameter $T_0/m\omega^2 a^2$ on M.

4. Dependence of guide eye tension on traveller mass

Figures 3*a*, 4*a* and 5*a* graph the dependence of guide eye tension parameter on traveller mass parameter over the range $0 \leq M \leq 1,000$, for a balloon of height $h = 10a$, lay-point radius $b = 0.5a$ and air drag parameter $p_0 = 4.0$. This range of M far exceeds the range $(50 \leq M \leq 150)$ that typically occurs in cotton spinning practice. In the next section a detailed discussion of the results for the larger range of M values will be given for this one example to display the full complexity of the mathematical problem. In subsequent sections the effect of variations in air drag p_0, balloon height and lay-point radius will be explored but the discussion there will be confined to the more restricted range of M values of practical interest.

(*a*) *Full results for a balloon of height* $h = 10a$ *and* $p_0 = 4.0$

(i) *Very small traveller mass:* $0 \leq M \leq 12$

As can be seen from figures 3*a* and 4*a* the $T_0/m\omega^2 a^2$ against M graph is multiple valued for certain ranges of traveller mass. For easy reference the various parts of the graph are labelled A, B, C and D as shown. The sections of the graph shown by the broken lines and which lie between branches A and B, B and C, and C and D (solid lines) will be referred to as branches A/B, B/C and C/D respectively. It will be assumed in the present discussion that the balloons corresponding to parameter values on these broken line branches are dynamically unstable. Such balloons are to be avoided in practice. This assumption seems reasonable on the following grounds: (i) the analogy between the present results and similar mathematical structures in parameter space that occur in certain nonlinear oscillation problems (cf. Jordan & Smith 1986, ch. 7); (ii) the oscillatory behaviour of an experimental balloon reported in Platt's Bulletin suggests the existence of such unstable branches.

A full investigation of the stability of these multiple solution regions will be the subject of a future investigation.

The first multiple solution region spans the range $0 \leq M < 2.734$, and typical balloon profiles for this region are shown in figure 3*b* for $M = 1.4$. The profile corresponding to the unstable branch A/B solution is shown by the broken line.

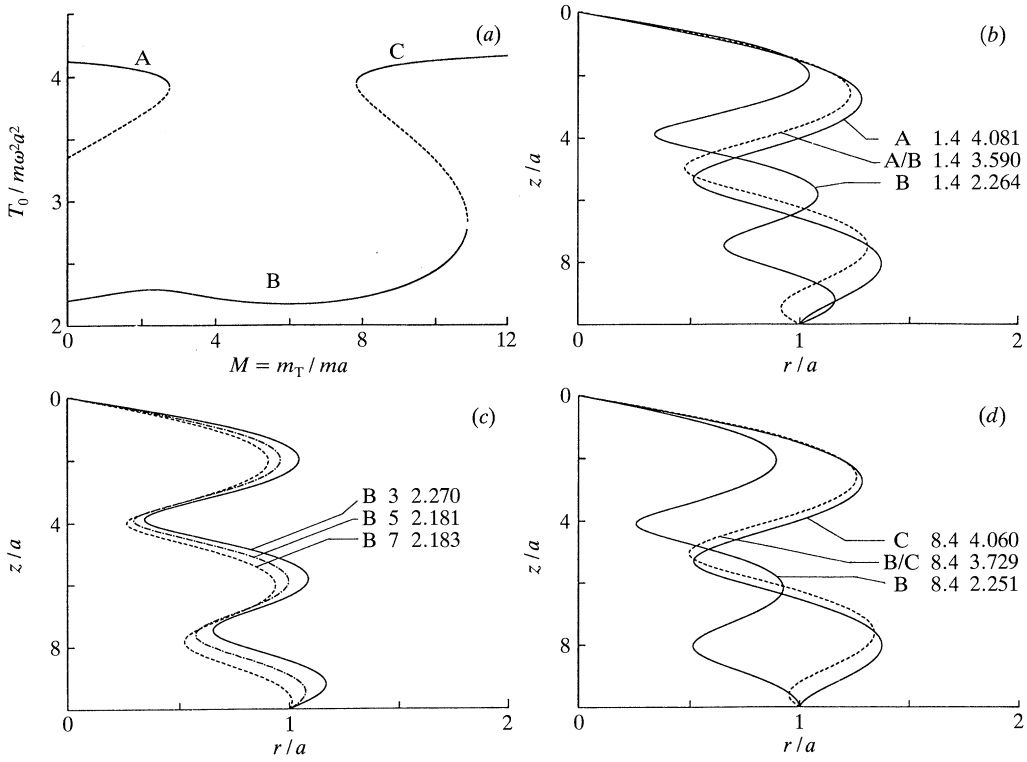

Figure 3. (*a*) Guide eye tension against very small values of traveller mass ($0 \leq M \leq 12$): $p_0 = 4.0$, $h = 10a$, $b = 0.5a$. (*b*) Typical balloon profiles for branch A and B overlap region ($0 < M < 2.734$) in (*a*). (*c*) Typical balloon profiles for branch B unique solution region ($2.734 < M < 7.810$) in (*a*). (*d*) Typical balloon profiles for branch B and C overlap region ($7.810 < M < 10.870$) in (*a*). In this and all other figures containing tables, the first column is the branch, the second is the value of M, and the third is the value of $T_0/m\omega^2 a^2$.

Experimentally one might expect to see a balloon profile that oscillates between the two and three loop balloon profiles shown by the solid curves in figure 3*b*.

In the range $2.734 < M < 7.810$ only unique branch B solutions exist and typical balloon profiles are shown in figure 3*c*.

The unstable branch B/C spans the range $7.810 < M < 10.870$ and typical balloon profiles are shown in figure 3*d*. The profile corresponding to the unstable branch is shown with a broken line.

(ii) *Balloon stability through the range of practical interest*

Figure 4*a* shows the guide eye tension against traveller mass curve through the range $0 \leq M \leq 80$. In the range $10.870 < M < 55.060$ only branch C solutions exist and typical balloon profiles are shown in figure 4*b*. The unstable branch C/D spans the range $55.060 < M < 56.930$ and typical balloon profiles are shown in figure 4*c*. The boundaries of the unstable regions have been determined accurate to three decimal places.

Taken together figure 4*b*, *c* show that as the traveller mass parameter is increased from $M = 10.0$ through the C–D transition to $M = 65$ the balloon

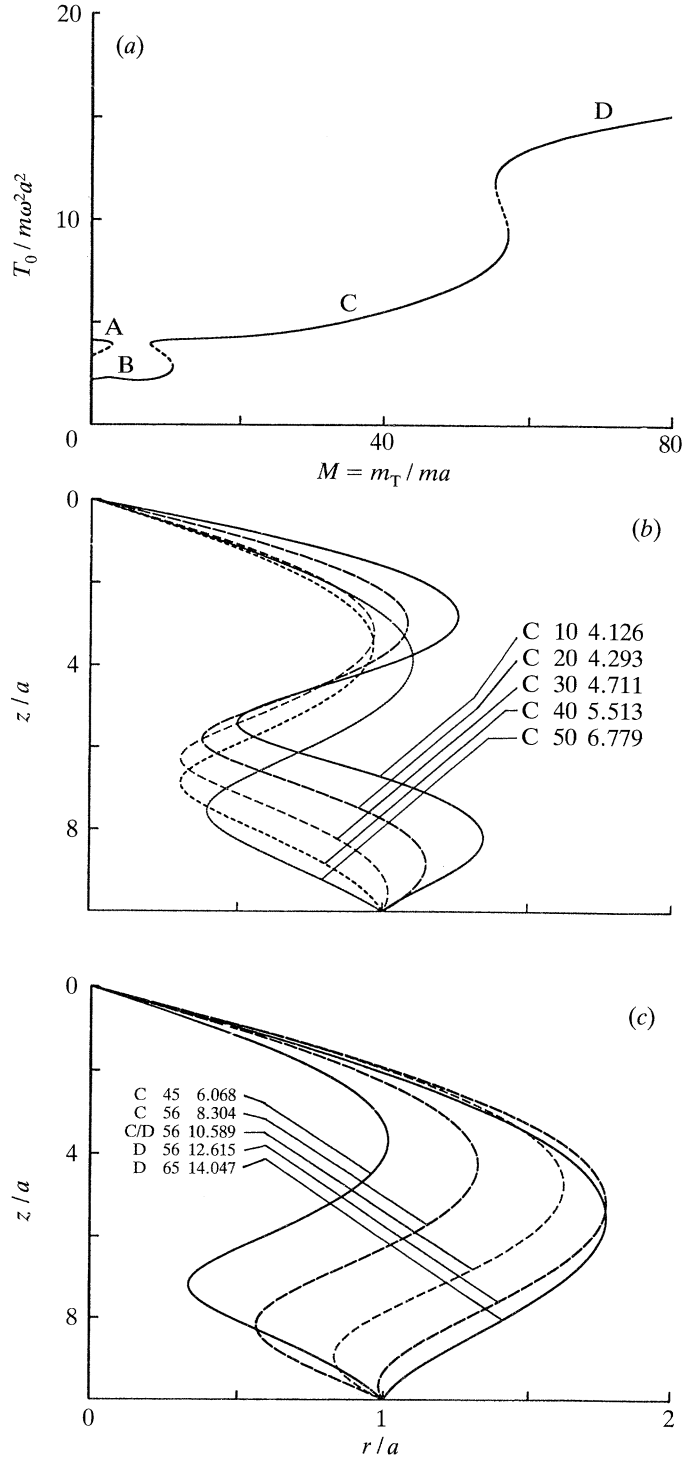

Figure 4. (*a*) Guide eye tension against traveller mass ($0 \leq M \leq 80$) through the C–D transition: $p_0 = 4.0$, $h = 10a$, $b = 0.5a$. (*b*) Typical balloon profiles for branch C unique solution region ($10.870 < M < 55.060$) in (*a*). (*c*) Typical balloon profiles for a range of M values through the C–D transition in (*a*).

PHILOSOPHICAL TRANSACTIONS OF THE ROYAL SOCIETY A MATHEMATICAL, PHYSICAL & ENGINEERING SCIENCES

profile changes from a stable two-loop shape to a stable single-loop shape. This is similar to the experimental result reported in Platt's Bulletin.

It is difficult to make a direct comparison of the present results with this experimental work because the experimental balloons were formed by replacing the ring and traveller mass by a disc attached to the spindle. The yarn from the guide eye was passed through a hole in the edge of the disc and from there through the spindle. The required tension was maintained by applying a weight to the bottom end of the yarn which was held stationary at the front roller nip. The photographs (figs 3 and 4 of Platt's Bulletin) show clearly what happens to the balloon as the spindle speed is increased from 6500 to 11 500 r.p.m. under a constant applied tension of 50 g mass. The balloon profile starts out in a stable single-loop configuration and then becomes unstable, oscillating rapidly between a single- and double-loop configuration, finally settling into a stable double-loop configuration at the higher spindle speed.

The balloon height is 330.2 mm and $h/a = 8.55$ (scaled off the photographs), which gives a ring radius of 38.6 mm. The yarn count was 59 tex (59 mg m^{-1}). From this data the change in the guide eye tension parameter corresponding to the change in spindle speed can be calculated: the increase of spindle speed from 6500 to 11 500 r.p.m. corresponds to a decrease of $T_0/m\omega^2a^2$ from 12.043 to 3.847. This corresponds quite well with the theoretical change in the value of this parameter in the transition from a stable point on branch D to a stable point on branch C. It is difficult to evaluate the effect of replacing the traveller by a driven disc.

Finally for the range $56.930 < M < 1000$ branch D solutions are unique. Typical balloon profiles are shown in figure 5*b*. In this region the guide eye tension parameter increases linearly with the traveller mass parameter and the balloon profiles have a single stable loop which becomes narrower and narrower with increasing tension and traveller mass.

As remarked at the beginning of this section the range of parameter M encountered in cotton spinning is roughly $50 < M < 150$. For a balloon of height 10 ring radii subject to an air drag coefficient $p_0 = 4.0$ this range includes the unstable transition region between branch C and D solutions. This transition will be referred to subsequently as the C–D transition and it is clear that its location on the M-axis is of considerable importance in the determination of optimal traveller mass. In the next section the dependence of this transition on air drag, balloon height and lay-point radius will be investigated in detail.

(*b*) *The* C–D *transition region:* $40 \leq M \leq 160$

In practice a multiple-loop balloon is called a collapsed balloon and, except in the case of collapsed balloon spinning, operating conditions that lead to multiple-loop balloons are to be avoided. It is well known that the cure is to use a sufficiently heavy traveller to insure the formation of a stable single-loop balloon. To achieve this condition in the example above a value of M greater than 60 should be used (figure 4*a*, *c*). It is clear then that the location of the C–D transition in the guide eye tension against traveller mass curve provides a lower bound on the operational value of M. Beyond the C–D transition $T_0/m\omega^2a^2$ increases approximately linearly with M (branch D, figure 5*a*) and the balloon profiles (figure 5*b*) remain single loop becoming narrower and narrower with increasing traveller mass and tension.

PHILOSOPHICAL TRANSACTIONS OF THE ROYAL SOCIETY A MATHEMATICAL, PHYSICAL & ENGINEERING SCIENCES

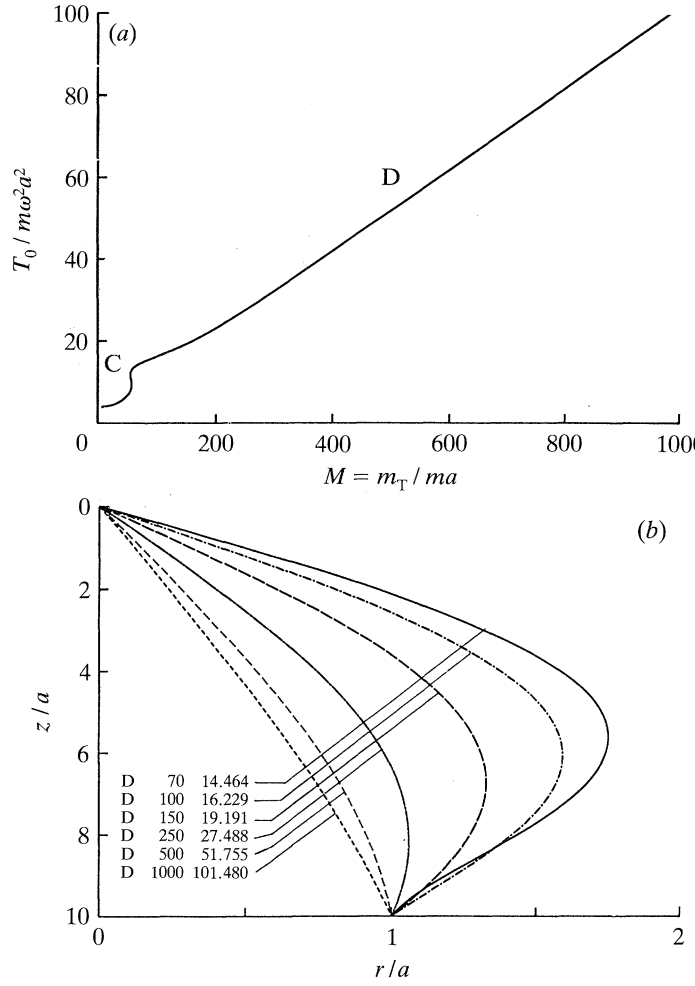

Figure 5. (*a*) Guide eye tension against traveller mass, branch C and D ($0 \leq M \leq 1000$): $p_0 = 4.0,\ h = 10a,\ b = 0.5a$. (*b*) Typical balloon profiles for branch D in (*a*).

Thus from a practical point of view the location of the C–D transition is a most important feature of these results. In the next three subsections the dependence of this transition on air drag, balloon height and bobbin radius will be examined in detail.

(i) *The effect of air drag*

The present model is based on the assumption that the balloon rotates in still air so that the yarn velocity relative to the air is identical with its absolute velocity relative to a stationary frame of reference. The effect of air entrainment due to the beating action of the balloon is ignored and indeed this would be difficult to model. It is also assumed that the air drag coefficient D_n in equation (2.3) is constant along the length of the yarn in the balloon and takes on the value appropriate to the yarn velocity at the point of maximum balloon radius (cf. Batra *et al.* 1989*b*). Finally the component of air drag force tangential to the yarn is neglected as the calculations of Kothari & Leaf (1979*a*) have shown that

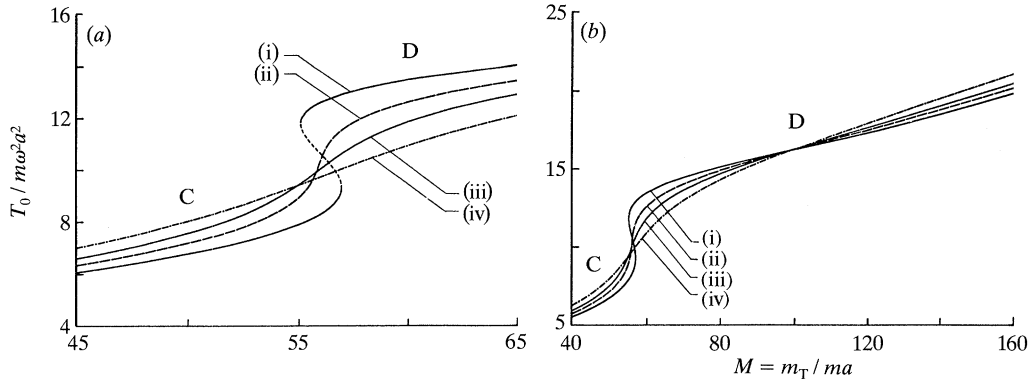

Figure 6. Guide eye tension against traveller mass: (*a*) ($45 \leq M \leq 65$) through the C–D transition; (*b*) ($40 \leq M \leq 160$) through the C–D transition and the anomalous region. p_0 has values: (i) 4.0, (ii) 5.0, (iii) 6.0 and (iv) 8.5; $h = 10a$, $b = 0.5a$.

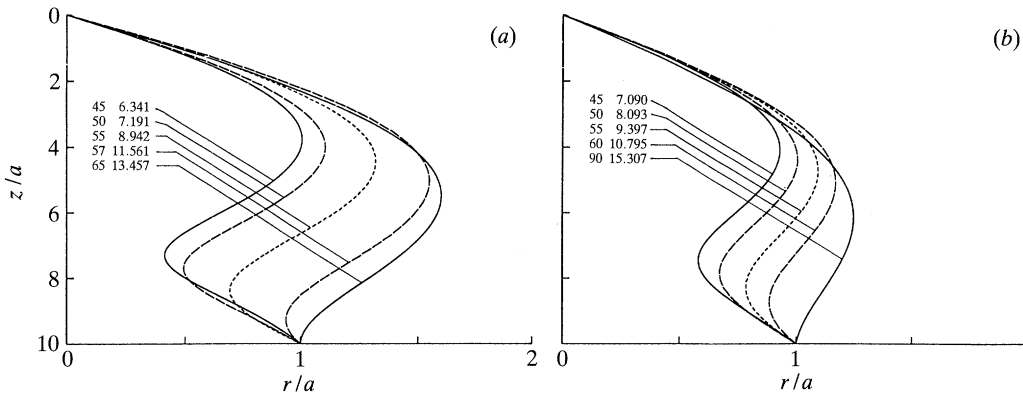

Figure 7. Typical balloon profiles through the C–D transition (figure 6): (*a*) $p_0 = 5.0$; (*b*) $p_0 = 8.5$.

its effect is negligible. Thus the air drag force is assumed to act in the direction normal to the yarn and to be proportional to the square of the magnitude of the normal component of yarn velocity.

With all of these qualifications firmly in mind the effect of variations in the value of p_0 on the C–D transition will now be considered.

Figure 6*a*, *b* shows the results. For $p_0 = 4.0$ the C–D transition consists of a triple solution region and the transition occurs via the unstable branch C/D shown by the broken line in figure 6*a*. For higher values of p_0 this region of instability disappears. Thus when $p_0 = 5.0$, although there is still a rapid increase in tension and change in balloon shape (figure 7*a*) through the C–D transition, the solutions remain unique and therefore stable. At a value of $p_0 = 8.5$ the transition from branch C to D is quite smooth and the change in balloon shape is more gradual (figure 7*b*).

Figure 6*b* shows that for the range $56 < M < 100$ (approximately) there is a seemingly anomalous dependence of tension on air drag. For this range of traveller mass an increase of air drag leads to a decrease in tension and therefore a decrease in power consumption. The reason is that air drag produces two contrary effects

on the balloon. On the one hand increasing the air drag reduces the maximum radius of the balloon which causes a decrease in the tension due to centripetal acceleration. On the other hand increasing the air drag force on the thread line increases the tension. In this anomalous region the former effect wins out over the latter for a small range of M. How dependent this curious effect is on the particular model of air drag used must be a matter for future investigation.

Finally observe that the location of the C–D transition range on the M axis is, for practical purposes, independent of the value of p_0 in the range $4.0 \leq p_0 \leq 8.5$.

(ii) *The effect of balloon height*

Figure 8*a–d* shows the effect of balloon height on the location of the C–D transition for a range of balloon heights from $h = 5a$ to $h = 15a$. All results in this subsection are for air drag parameter $p_0 = 4.0$. For a balloon of height $h = 5a$ the C–D transition has moved out of the range of current practical interest ($50 \leq M \leq 150$) and the curve for this balloon height shown in figure 8*a* is wholly branch D. The corresponding balloon profiles are shown in figure 8*b*.

As the balloon height increases the transition region moves to higher values of M and when $h = 12a$ the solutions remain unique through the transition. For larger values of h the transition between region C and D becomes less abrupt. Balloon profiles for the case $h = 14a$ are shown in figure 8*c*.

Figure 8*d* shows the continuation of the curves in figure 8*a* to a value of $M = 600$ and it can be seen that the curves converge to a set of closely spaced almost parallel straight lines.

(iii) *The effect of bobbin radius*

As each layer of thread (cf. § 5) is wound onto the bobbin the lay-point radius slowly decreases, starting almost equal to the ring radius at the bottom of the conical chase and finishing equal to the core tube radius. This gives rise to substantial changes in tension as can be seen in figure 9*a*. As the bobbin radius increases the guide eye tension decreases and the C–D transition moves to higher values of M and becomes less abrupt so that the unstable region is smoothed out. The curve for $b = a$ is shown as this provides a lower bound on the results and in practice bobbins are wound to a radius as close to the traveller ring as possible. As M increases through the transition region the balloon profiles change from two-loop to single-loop shapes (figure 9*b*).

This brings the account of the theory of free balloon ring spinning to an end. Before proceeding to an account of the theory of spinning with control rings it seems appropriate to comment on some of the practical consequences of the theory so far.

5. Practical consequences for free balloon spinning

The *cop* is the characteristic form of package produced by the ring spinning machine (figure 10*a*). The yarn is wound on a wood, paper, or plastic tube that fits snuggly over the spindle. The shape of the cop is built up by the superposition of many conical layers. Each layer is composed of a main winding and a cross winding (figure 10*b*). The main winding is formed during the slow rise of the ring rail while the open cross winding forms during its more rapid descent. The cross windings thus separate the main windings from each other and prevent complete

PHILOSOPHICAL TRANSACTIONS OF THE ROYAL SOCIETY A MATHEMATICAL, PHYSICAL & ENGINEERING SCIENCES

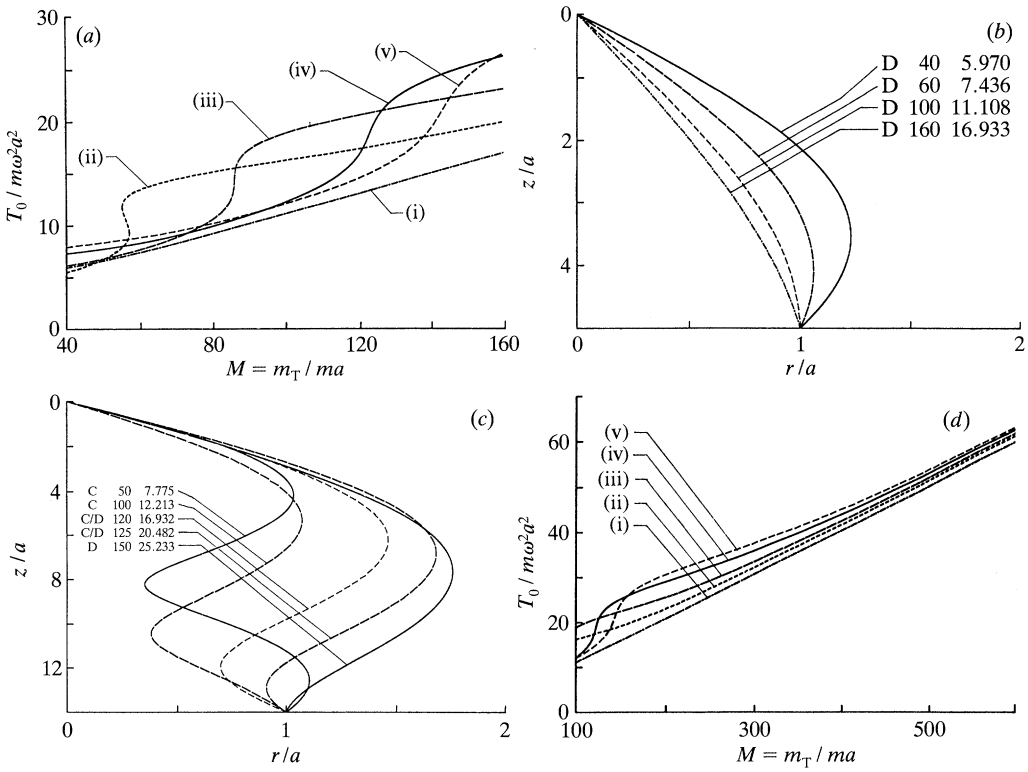

Figure 8. (*a*) Guide eye tension against traveller mass ($40 \leq M \leq 160$) dependence on balloon height. (*b*) Typical balloon profiles for a range of M values on branch D (figure 8*a*): $h = 5a$. (*c*) Typical balloon profiles through the C–D transition (figure 8*a*): $h = 14a$. (*d*) Guide eye tension against traveller mass ($100 \leq M \leq 600$) dependence on balloon height. (*a*)–(*d*) $p_0 = 4.0$, $b = 0.5a$. Values of h/a in (*a*) and (*d*) are (i) 5, (ii) 10, (iii) 12, (iv) 14, (v) 15.

layers from being pulled off during unwinding. Superposed on this oscillatory motion of the ring rail that builds the conical layers is a gradual rise of the ring rail from the bottom to the top of the tube called the lift of the ring rail.

Thus there is a considerable change in balloon height during the building sequence from the first to the last layer of yarn. If a stable single-loop balloon is to be achieved without changing the traveller mass during the process it is necessary to choose an M value above the location of the C–D transition of the greatest balloon height and lay-point radius. For example, if the greatest balloon height is $h = 14a$, a value of $M > 150$ (figures 8 and 9) would ensure stable single balloon operation during the whole building sequence. As the balloon height decreases the tension decreases (if the spindle speed is kept constant).

For a given balloon height, yarn count and traveller mass, the term $T_0/m\omega^2 a^2$ is constant and so guide eye tension is proportional to the square of the angular speed of the traveller (which is approximately the same as the spindle speed). Thus, to some extent, variations in spindle speed can be used to control the change in tension due to the lift of the ring rail during the building sequence.

The tension also changes during the winding of each conical yarn layer. This is in part due to the change in balloon height but more importantly it is due to the change in radius of the lay point from the bottom to the top of the layer. This

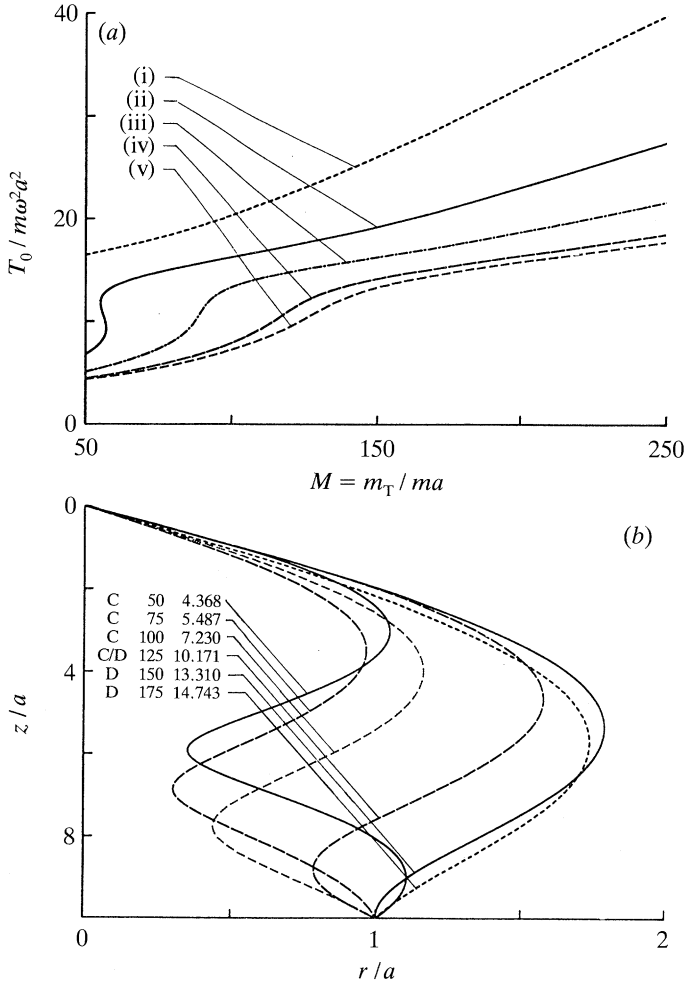

Figure 9. (*a*) Guide eye tension against traveller mass ($50 \leq M \leq 250$) dependence on bobbin radius: $p_0 = 4.0$, $h = 10a$; values of b are (i) $0.3a$, (ii) $0.5a$, (iii) $0.7a$, (iv) $0.9a$, (v) $1.0a$. (*b*) Typical balloon profiles through the C–D transition (figure 9*a*): $p_0 = 4.0$, $h = 10a$, $b = a$.

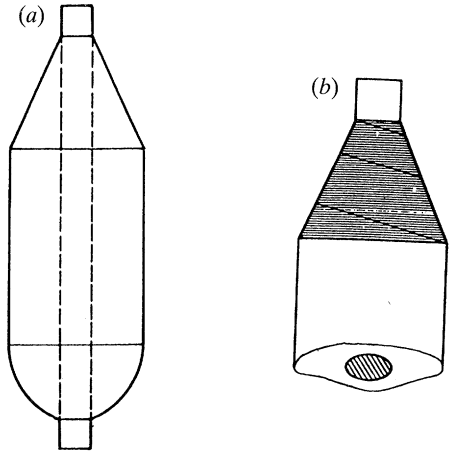

Figure 10. (*a*) The cop form. (*b*) Main windings and cross windings.

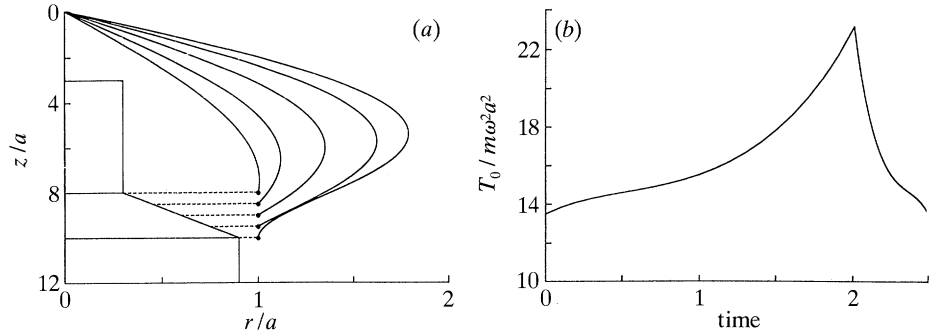

Figure 11. (*a*) Change in balloon profile during winding on the conical surface of the cop ($M = 150$, $p_0 = 4.0$). (*b*) Change in guide eye tension during winding on the conical surface of the cop ($M = 150$, $p_0 = 4.0$).

tension variation could also be reduced by varying the spindle speed during the traverse of the ring rail up and down the conical chase.

(*a*) *Simulation of a traverse up and down the conical chase*

The programs developed to obtain the above results have been used to simulate the variation in balloon shape and guide eye tension as one layer of yarn is wound on the conical surface of the cop ($p_0 = 4.0$).

The balloon height and lay-point radius at the bottom of the traverse are $h = 10a$ and $b = 0.9a$, and at the top of the traverse $h = 8a$ and $b = 0.3a$. Figure 11*a* shows the change in balloon profile and figure 11*b* shows the variation in guide eye tension parameter which varies from a minimum of 13.496 to a maximum value of 23.168.

The value of $M = 150$ was used for this calculation and in figure 11*a* it can be seen that the balloon profile at the bottom of the cone is just developing a neck ($r'(s_1) = 0$). For all the other profiles $r'(s_1) < 0$. If cops are to be wound as full as possible the traveller mass must be chosen so that the highest balloon at its maximum radius is just forming a neck (i.e. $r'(s_1; h_{\max}, b_{\max}) = 0$). This condition has been used to compute the minimum traveller mass against balloon height curves shown in figure 12*a*. The equation for computing minimum traveller mass given by de Barr & Catling (eqn 15.3, p. 218) is also plotted. In the notation of this paper their equation is

$$M = m_{\mathrm{T}}/ma = 0.9449(h/a)^2.$$

Surprisingly, the theoretical curves give a more conservative estimate of minimum traveller mass than this equation. The guide eye tensions corresponding to these minimum traveller mass conditions are plotted in figure 12*b*. Note the anomalous dependence of tension on air drag p_0 for $h < 8a$ which corresponds to $M < 100$ as discussed in § 4 *b*(i).

Finally note that there is no theoretical restriction on the speed of the traveller (approximately equal to the spindle speed) as ω does not occur explicitly in the theoretical results. It is hidden in the denominator of the dimensionless guide eye tension parameter. The maximum practical value of ω is restricted by the amount of traveller wear that can be tolerated in a particular spinning operation. This is determined by considerations of economic machine operation. Although

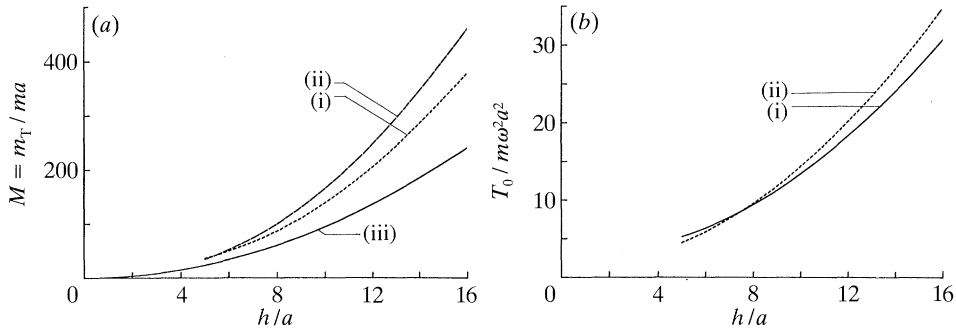

Figure 12. (a) Minimum traveller mass against balloon height for free balloon spinning; $b = 0.9a$; (i) $p_0 = 4.0$, (ii)$p_0 = 8.0$, (iii) de Barr & Catling (eqn (15.3)). (b) Guide eye tension against balloon height for free balloon spinning with minimum traveller mass (figure 12a); $b = 0.9a$; (i) and (ii) as (a).

such considerations are outside the scope of this paper it is appropriate to note that frictional wear will be closely related to the normal pressure between the traveller and the ring which can be computed from equations (2.8)–(2.10).

Once the value of $M = m_T/ma$ is chosen to ensure that a stable single-loop balloon is formed during the whole of the spinning cycle the spindle speed can be varied to help minimize tension variations.

Most modern ring spinning machines use control rings to restrict balloon radius and reduce yarn tensions at large balloon heights. In the next section the effect of a control ring of radius a, placed half way up a balloon of total height $h = 10a$, will be investigated.

6. The effect of balloon-control rings

In the first part of this section the mathematical formulation will be modified to take account of the constraint of a balloon-control ring on the balloon. In the second part a numerical procedure for calculating controlled balloon profiles and tensions will be described and the effect on the $T_0/m\omega^2a^2$ against M curve of a single control ring of radius a half way up a balloon of height $h = 10a$ will be given for $p_0 = 4.0$. It is not the purpose in this paper to give a complete investigation of the parameter space of ring spinning with control rings. This will be taken up in subsequent papers.

(a) *Mathematical formulation for a balloon-control ring*

The control ring will be assumed to be a point constraint on the yarn in the balloon that exerts a point force on the yarn at distance $s = s_c$ ($z(s_c) = h_c$) along the thread line from the guide eye†. Equation (2.25) with inextensibility condition (2.6) still describes the motion of the thread line between the guide eye and the control ring and between the control ring and the traveller ring. The boundary conditions at the guide eye and the traveller are unchanged. The tension equation

† Throughout this section the dimensionless variables defined in equation (2.18) will be used. The overbars will be omitted.

(2.27) is still valid if the tension in the yarn is assumed to be continuous across the control ring.

The new conditions required are the obvious geometrical constraints at $s = s_c$:

$$r(s_c) = c, \quad z(s_c) = h_c, \tag{6.1}$$

where c is the ratio of the radius of the control ring to the radius of the traveller ring and h_c is the ratio of the vertical distance between the guide eye and the control ring to the radius of the traveller ring. The coordinate $\theta(s)$ must also be continuous. These conditions must be taken together with a dynamic condition to allow for the force the control ring exerts on the yarn. This latter condition is derived as follows.

Let the point force the control ring exerts on the yarn be given by

$$\boldsymbol{F}_c = \left\{ F_r \boldsymbol{e}_r + F_z \boldsymbol{k} - \mu_c \left(\sqrt{F_r^2 + F_z^2} \right) \boldsymbol{e}_\theta \right\} \delta(s - s_c), \tag{6.2}$$

where μ_c is the coefficient of friction between the yarn and the ring and $\delta(s - s_c)$ is the Dirac delta function. As is usual it is assumed that the direction of the frictional force the (finite) control ring exerts on the yarn is opposite to the direction of the velocity of the yarn element sliding over the surface of the control ring, i.e. in the direction of $-\boldsymbol{v} = -\boldsymbol{k} \wedge \boldsymbol{R} = -r\boldsymbol{e}_\theta$ (cf. equation (2.19_3)). So the direction of this frictional force is $-\boldsymbol{e}_\theta$ and this is consistent with the assumption that the yarn speed V through the balloon is very small compared with the linear speed, ωa, of the traveller (see also discussion in Krause & Soliman (1989)).

The equation of motion (2.25) can now be applied to the whole of the yarn between the guide eye and the traveller if this additional concentrated force term is added to the right side of equation (2.25):

$$\begin{aligned} \boldsymbol{k} \wedge (\boldsymbol{k} \wedge \boldsymbol{R}) = {} & \frac{\mathrm{d}}{\mathrm{d}s} \left(T \frac{\mathrm{d}\boldsymbol{R}}{\mathrm{d}s} \right) + \tfrac{1}{16} p_0 |\boldsymbol{v}_n| \boldsymbol{v}_n \\ & + \left\{ F_r \boldsymbol{e}_r + F_z \boldsymbol{k} - \mu_c \left(\sqrt{F_r^2 + F_z^2} \right) \boldsymbol{e}_\theta \right\} \delta(s - s_c). \end{aligned} \tag{6.3}$$

This equation must now be integrated from $s = s_c^-$ to $s = s_c^+$ to yield a point condition at the control ring. The result is

$$(T_0 - \tfrac{1}{2}c^2) \left| \frac{\mathrm{d}\boldsymbol{R}}{\mathrm{d}s} \right|_{s_c^-}^{s_c^+} = - \left\{ F_r \boldsymbol{e}_r + F_z \boldsymbol{k} - \mu_c \left(\sqrt{F_r^2 + F_z^2} \right) \boldsymbol{e}_\theta \right\}, \tag{6.4}$$

where account has been taken of the continuity of the yarn coordinates, and the yarn tension and the air drag term have been assumed continuous across the ring. The cylindrical coordinate components of this last equation are:

$$\left.\begin{aligned} (T_0 - \tfrac{1}{2}c^2)[r'(s_c^+) - r'(s_c^-)] &= -F_r, \\ (T_0 - \tfrac{1}{2}c^2)[c\theta'(s_c^+) - c\theta'(s_c^-)] &= \mu_c \sqrt{F_r^2 + F_z^2}, \\ (T_0 - \tfrac{1}{2}c^2)[z'(s_c^+) - z'(s_c^-)] &= -F_z. \end{aligned}\right\} \tag{6.5}$$

It will be assumed (cf. Ghosh *et al.* 1992) that the frictional interaction between the yarn and the balloon control ring is made negligible by aerodynamic lubrication. Thus the right side of equation (6.5_2) is zero and the dynamic condition to

be used in the solution of the balloon equations reduces to the continuity of θ' across the control ring. Equations (6.5_1) and (6.5_3) determine the normal force between the yarn and the control ring once the jump in r' and z' has been determined from the solution to the balloon equations. Note also that these jumps are not independent for, by the inextensibility condition (2.6),

$$\left| r'^2 + z'^2 \right|_{s_c^-}^{s_c^+} = 0.$$

(*b*) *Method of numerical solution*

The numerical solution of this problem is achieved in three main steps. The solutions of the differential equations appropriate to the balloon between the guide eye and control ring, and the balloon between the control ring and the traveller ring must first be obtained. These two solutions must then be fitted together at the control ring. For a given choice of M the detailed procedure is as follows.

1. Since θ' is continuous across the control ring first assume a trial value of $\theta'(s_c) = \theta'_{\text{trial}}$.

2. Use the shooting method outlined in § 3 to solve for the balloon shape between the guide eye and control ring subject to boundary conditions (2.21) at the guide eye and $r(s_c) = c$, $z(s_c) = h_c$ and $\theta'(s_c) = \theta'_{\text{trial}}$ at the control ring. This will also determine corresponding values of $T_0 = t_1$, $r'(0)$, s_c and the coordinate $\theta(s_c) = \theta_c$.

3. Now use the shooting method to solve for the balloon shape between the control ring and the traveller subject to boundary conditions $r(s_c) = c$, $\theta(s_c) = \theta_c$, $\theta'(s_c) = \theta'_{\text{trial}}$ and $z(s_c) = h_c$ at the control ring and conditions (2.22) and (2.23) at the traveller. This calculation will also give rise to values of $T_0 = t_2$, $r'(s_c)$ and the total length of yarn s_l between the guide eye and the traveller.

4. The solutions found in steps 2 and 3 satisfy the conditions for the geometrical continuity of the thread line at the control ring and also the boundary conditions at the guide eye and the traveller. However, the guide eye tensions t_1 and t_2 will not in general be equal and their difference will depend on the trial value θ'_{trial}. A Newton–Raphson type iteration scheme is used to find the value of θ'_{trial} for which $t_1 = t_2$.

The results of such a calculation are shown in figure 13*a*, *b*. Figure 13*a* shows that the effect of the control ring in this case is to stabilize the two-loop balloon through the C–D transition in the practical range of M. At a sufficiently high value of M the yarn will loose contact with the control ring and a single-loop free balloon will form. In figure 13*b*, which shows typical balloon profiles corresponding to figure 13*a*, it can be seen that this last condition is almost reached when $M = 150$.

7. Concluding remarks

This paper has been mainly concerned with free balloon spinning (without control rings). The relation between guide eye tension and traveller mass has been explored in some detail and an important transition region in this dependence has been identified. This is the range of (increasing) traveller mass values over which the balloon profiles change from stable two-loop shapes to stable single-

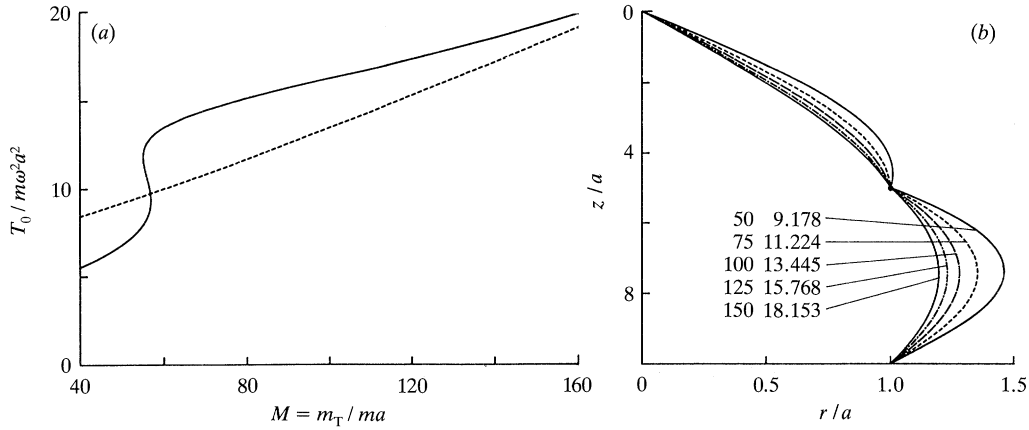

Figure 13. (*a*) Guide eye tension against traveller mass for the range ($40 \leq M \leq 160$). Comparison of free balloon spinning (————) and spinning with a control ring (– – – –). (*b*) Typical balloon profiles for controlled spinning corresponding to the traveller mass range in (*a*); $p_0 = 4.0$, $h = 10a$, $b = 0.5a$.

loop shapes. For some parameter values this transition is made through a range of traveller mass values for which the balloon shapes are unstable.

The dependence of this transition region on bobbin radius, balloon height and air drag was also examined in detail. The practical application of the theory was discussed and theoretical minimum traveller mass curves were produced. The results of a simulation of one traverse of the ring rail up and down the conical chase of a cop-structured bobbin were presented. In § 6 the theory was modified to allow for the presence of a control ring and results that show the effect of the control ring on the guide eye tension, traveller mass dependence were presented.

Most of the discussion has been confined to the range of traveller mass ($40 \leq M \leq 160$) of interest to cotton spinners. The existence of stable multi-loop balloon solutions at very small values of M (branches B and C, figures 3*a* and 4*a*) and correspondingly low tensions may be of practical interest for the low tension spinning of very fragile yarns. A more complete investigation of this range of M values will be taken up in a future paper along with the investigation of the stability of the solutions on the multi-valued branches of the guide eye tension against traveller mass curves.

The effect of control rings, which has only been touched on in this paper, must also be a matter for further investigation.

I thank Dr Nigel Johnson of the School of Fibre Science and Technology, at The University of New South Wales, for his helpful advice during the course of this investigation, and for the loan of various books, reprints and other material from his personal library. The research reported in this paper is part of an on-going research programme into yarn ballooning being carried outin collaboration with Professor S. K. Batra and Professor T. K. Ghosh at the College of Textiles, North Carolina State University, Raleigh. This research is supported in part by the U.S. National Textile Center.

Appendix A. Equations of motion for the yarn in the ring spinning balloon

In this appendix the three components of the equation of motion for the yarn in the ring spinning balloon, equation (2.25), are given with respect to both cylindrical and cartesian coordinate systems rotating with the angular velocity of the traveller. The leading terms in the power series expansions (valid near the guide eye) of the solutions to each of these sets of component equations are also given.

(a) *In cylindrical coordinates*

With respect to cylindrical coordinates (r, θ, z) the components of equation (2.25) are:

$$T\left(r'' - r\theta'^2\right) = -r + rr'^2 - \tfrac{1}{16}p_0(r^2r'\theta')v_n, \tag{A 1}$$

$$T\left(2r'\theta' + r\theta''\right) = r^2r'\theta' + \tfrac{1}{16}(p_0/r)(v_n)^3, \tag{A 2}$$

$$Tz'' = rr'z' - \tfrac{1}{16}p_0(r^2\theta'z')v_n, \tag{A 3}$$

where $0 \leq s \leq s_1$, $(\ )' \equiv \mathrm{d}(\ )/\mathrm{d}$, normal speed $v_n = r\sqrt{r'^2 + z'^2}$, and the tension is $T = T_0 - \frac{1}{2}r^2$. The inextensibility condition is

$$(r')^2 + (r\theta')^2 + (z')^2 = 1, \tag{A 4}$$

and T_0 is the tension in the balloon at the guide eye.

(i) *Series solution at the guide eye*

The leading terms in the power series expansions of the solutions of equations (A 1)–(A 4) in the neighbourhood of the origin of coordinates at the guide eye are:

$$r(s) = r_1 s + \cdots, \quad \theta(s) = \frac{p_0 r_1}{192T_0}s^3 + \cdots, \quad z(s) = \{1 - r_1\}^{1/2}s + \cdots, \tag{A 5}$$

where $r_1 = r'(0)$ and T_0, the initial slope and guide eye tension, must be specified to obtain a trial solution of the initial value problem for use in the shooting method algorithm used to solve the two-point boundary value problem.

(b) *In cartesian coordinates*

With respect to cartesian coordinates (x, y, z) the components of equation (2.25) are:

$$Tx'' = -x + (xx' + yy')x' + \tfrac{1}{16}p_0[(yx' - xy')x' - y]v_n, \tag{A 6}$$

$$Ty'' = -y + (xx' + yy')y' + \tfrac{1}{16}p_0[(yx' - xy')y' + x]v_n, \tag{A 7}$$

$$Tz'' = (xx' + yy')z' + \tfrac{1}{16}p_0[(yx' - xy')z']v_n, \tag{A 8}$$

where the normal speed is $v_n = \sqrt{(xx' + yy')^2 + z'^2(x^2 + y^2)}$, the tension is $T = T_0 - \frac{1}{2}(x^2 + y^2)$, and the inextensibility condition is

$$(x')^2 + (y')^2 + (z')^2 = 1. \tag{A 9}$$

(i) *Series solution at the guide eye*

The power series expansions (including terms up to order s^4) of the solutions of equations (A 6)–(A 8) in the neighbourhood of the origin of coordinates at the guide eye are:

$$\left.\begin{aligned} x(s) &= x_1 s + \frac{x_1 {z_1}^2}{6T_0} s^3 - \frac{p_0 y_1 \sqrt{{x_1}^2 + {y_1}^2}}{192 T_0} s^4 + \cdots, \\ y(s) &= y_1 s + \frac{y_1 {z_1}^2}{6T_0} s^3 + \frac{p_0 x_1 \sqrt{{x_1}^2 + {y_1}^2}}{192 T_0} s^4 + \cdots, \\ z(s) &= z_1 s - \frac{z_1 (1 - {z_1}^2)}{6T_0} s^3 + \cdots, \end{aligned}\right\} \tag{A 10}$$

where $x_1 = r'(0)$, $y_1 = y'(0)$, ${z_1}^2 = 1 - {x_1}^2 - {y_1}^2 = [z'(0)]^2$ and T_0, the initial slopes and guide eye tension, must be specified to obtain a trial solution of the initial value problem for use in the shooting method algorithm used to solve the two-point boundary value problem.

References

Batra, S. K., Ghosh, T. K. & Zeidman, M. I. 1989*a* *Text. Res. J.* **59**, 309–317.

Batra, S. K., Gosh, T. K. & Zeidman, M. I. 1989*b* *Text. Res. J.* **59**, 416–424.

Batra, S. K., Gosh, T. K., Zeidman, M. I. & Dua, B. E. 1989*c* *Dynamic analysis of the ring spinning process: a progress report.* Raleigh: College of Textiles, NCSU.

Blumen, G. W. & Kumei, S. 1989 *Symmetries and differential equations.* Springer-Verlag.

Bridgeman, P. W. 1939 *Dimensional analysis*, 2nd edn. Yale University Press.

de Barr, A. E. & Catling, H. 1965 *The principles and theory of ring spinning. Manual of cotton spinning* (ed. F. Charnley & P. V. Harrison), vol. 5. Manchester and London: Butterworths Press.

Crank, J. 1953 *Text. Res. J.* **23**, 266–276.

Fraser, W. B. 1992 *J. Text. Inst.* **83**, 603.

Fraser, W. B., Ghosh, T. K. & Batra, S. K. 1992 *Proc. R. Soc. Lond.* A **436**, 479–498.

Ghosh, T. K., Batra, S. K., Dua, B. & Zeidman, M. I. 1992 *An integrated approach to dynamic analysis of the ring spinning process. Part III. The effect of coefficients of friction and the balloon control rings.* Vol. 47, Textile Praxis International.

Jordan, D. W. & Smith, P. 1986 *Nonlinear ordinary differential equations.* Oxford University Press.

Kevorkian, J. & Cole, J. D. 1981 *Perturbation methods in applied mathematics.* New York and Berlin: Springer-Verlag.

Klein, W. 1987 *Manual of textile technology: short-staple spinning series* (ed. H. Stalder), vol. 4: A practical guide to ring spinning. Manchester: The Textile Institute.

Kothari, V. K. & Leaf, G. A. V. 1979 *J. Text. Inst.* **70**, 89–94; 95–105.

Krause, H. W. & Soliman, H. A. 1989 *Melliand Textilberichte* **70**, 159–162.

Lisini, G. G., Nerli, G. & Rissone, P. 1981 *J. Engng Industry* **103**, 424–430.

Lüdicke, A. 1881 *Dingler's Polytechnisches J.* **242**, 334.

Nerli, G., Citti, P., Rissone, P., Bona, M. & Cerretini, A. 1980 In *Proc. 6th Inst. Wool Textile Research Conf. Pretoria*, vol. 3, pp. 607–617.

Padfield, D. G. 1958 *Proc. R. Soc. Lond.* A **245**, 382–407.

Platt 1955 Optimal spinning. *Platt's Bull.* **9**(8), 219–236.

Press, W. H., Flannery, B. P., Teukolsky, S. A. & Vetterling, W. T. 1986 *Numerical recipies: the art of scientific computing.* Cambridge University Press.

PHILOSOPHICAL TRANSACTIONS OF THE ROYAL SOCIETY A MATHEMATICAL, PHYSICAL & ENGINEERING SCIENCES

Sedov, L. I. 1959 *Similarity and dimensional methods*, 4th edn. New York: Academic Press.
Shantong, Z. 1987 *J. Chinese Textile University* **13**, 45–50.

Received 6 December 1991; accepted 3 June 1992

PHILOSOPHICAL TRANSACTIONS OF THE ROYAL SOCIETY A MATHEMATICAL, PHYSICAL & ENGINEERING SCIENCES